

Magnetic and Superconducting Ordering at LaAlO₃/SrTiO₃ Interfaces

Lukasz Fidkowski,¹ Hong-Chen Jiang,^{1,2,3} Roman M. Lutchyn,¹ and Chetan Nayak^{1,4}

¹Station Q, Microsoft Research, Santa Barbara, CA 93106-6105, USA

²Kavli Institute for Theoretical Physics, University of California, Santa Barbara, CA 93106

³Center for Quantum Information, IIS, Tsinghua University, Beijing, 100084, China

⁴Department of Physics, University of California, Santa Barbara, CA 93106

(Dated: compiled November 28, 2021)

We formulate a model for magnetic and superconducting ordering at LaAlO₃/SrTiO₃ interfaces containing both localized magnetic moments and itinerant electrons. Though these both originate in Ti 3d orbitals, the former may be due to electrons more tightly-bound to the interface while the latter are extended over several layers. Only the latter contribute significantly to metallic conduction and superconductivity. In our model, the interplay between the two types of electrons, which is argued to be ferromagnetic, combined with strong spin-orbit coupling of the itinerant electrons, leads to magnetic ordering. Furthermore, we propose a model for interfacial superconductivity, consisting of random superconducting grains in the bulk STO driven, via coupling to the interface conduction band, towards long-ranged or quasi-long-ranged order. Most interestingly, the magnetic order and strong spin orbit coupling can lead in this manner to unconventional interfacial superconductivity, yielding a possible realization of Majorana physics.

I. INTRODUCTION

It was recently discovered that, although LaAlO₃ and SrTiO₃ are both insulators, the interface between them is metallic¹. Furthermore, the electrons at this interface have shown a variety of remarkable properties, including magnetism²⁻⁵ and superconductivity⁶. Magnetism and superconductivity often appear in the phase diagram of strongly-correlated materials, where they compete. However, it is very unusual for them to occur simultaneously, which appears to be the case at the LAO/STO interface^{4,5,7}. A basic question, then, is whether the same electrons are exhibiting both superconductivity and magnetism or if, instead, there is a precise sense in which there are two species of electrons – two different electronic bands, for instance – one of which is superconducting and the other of which is magnetic. In the former case, the superconductivity must be exotic, perhaps *p*-wave superconductivity or a Fulde-Ferrel-Larkin-Ovchinnikov (FFLO) state^{8,9}. This would contradict the conventional wisdom that the interface electrons are simply exhibiting the superconductivity of doped SrTiO₃, which is presumed to be a phonon-mediated *s*-wave superconductor.

The experiments that reveal interesting magnetic behavior fall into two classes, those which deduce magnetism from transport and those which attempt to measure it more directly. The former include experiments that observe hysteresis in the electrical resistance as a function of magnetic field^{2,3}, which show that there is a magnetic field-driven first-order phase transition which has a large effect on the resistance. A magnetic transition is the most natural hypothesis. These signatures are found up to temperatures in excess of 200K. The latter include a torque magnetometry measurement⁴ that shows that a field as small as a few milliTesla leads to a large magnetization, approximately $0.3 \mu_B$ per interface unit cell. This implies that the system has ferromagnetic domains which become aligned by even a very small field. This experiment shows that the magnetic moment, which points in the plane, has an onset temperature that is at least as high as 40K and persists below the superconducting T_c . Finally, scanning SQUID

magnetometry⁵ finds micron sized ferromagnetic domains in a paramagnetic background. From their estimates, most of the interfacial electrons which are predicted by polar catastrophe arguments¹ are paramagnetic. An order of magnitude smaller number of electrons are in ferromagnetic regions, and a two orders of magnitude smaller number of electrons are in superconducting regions. There does not appear to be any correlation between the magnetic and superconducting regions (unless there is spatial segregation in the *z* direction), which implies that magnetism in a region does not prevent superconductivity from occurring in that region, counter to conventional wisdom. Taken together, these experiments constitute strong evidence that there are ferromagnetic domains at the LAO/STO interface that strongly affect normal state transport and are also present in the superconducting state.

Since neither LAO nor STO is magnetic, there is clearly a puzzle here: what is the cause of (at least local) ferromagnetism at their interface? It has been suggested that there is a narrow band at the interface¹⁰ which gives rise to itinerant electron ferromagnetism. Alternatively, the magnetism may be due to localized electrons which don't participate in the metallic (or superconducting) behavior. To make matters even less clear, there is evidence^{11,12} for strong spin-orbit coupling due to the broken inversion symmetry of the interface¹³ (Rashba spin-orbit coupling), which would ordinarily be antithetical to a uniform ferromagnetic moment.

An equally vexing problem is how ferromagnetism can co-exist with superconductivity¹⁴. Even if there were a sense in which different electronic bands were becoming ferromagnetic and superconducting, one would expect the magnetic moments of the former electrons to destroy superconductivity in the latter. One possibility is that the system is in an inhomogeneous superconducting state, e.g. the FFLO state, as suggested in Ref. 15. Or, one could imagine larger scale inhomogeneity, so that the system breaks up into domains, some of which are superconducting while others are ferromagnetic. But the ferromagnetic moment would be anti-correlated with superconductivity in either type of inhomogeneous state. For instance, in the FFLO state, the system forms superconduct-

ing stripes, separated by magnetic ones. This disagrees with the experimental finding of Ref. 5. Therefore, it is natural to consider, instead, a p -wave superconducting state, but this begs question of what the superconducting mechanism is. Presumably, p -wave superconductivity must be due to electron-electron interactions, rather than the electron-phonon coupling. Thus, superconductivity at the LAO/STO interface is a puzzle. It is generally assumed that it is related to superconductivity in doped STO, but this assumption does not provide any clues to how it can coexist with ferromagnetism.

In this paper, we present a physical picture for magnetism and superconductivity at the LAO/STO interface. Density functional theory calculations show that there are t_{2g} bands at the interface, corresponding to Ti $3d$ orbitals, with d_{xy} and $d_{xz,yz}$ symmetry respectively^{10,16}. We hypothesize that the d_{xy} band forms a band of localized electrons which accounts for most of the charge required by the ‘polar catastrophe’¹⁷. According to our picture, the $d_{xz,yz}$ bands form metallic bands of itinerant electrons at the interface. Coulomb interactions between localized and itinerant electrons generates a ferromagnetic interaction between them, thereby leading to a ferromagnetic Kondo model – but one in which the itinerant electrons have significant Rashba spin-orbit coupling. By analyzing a spin-orbit-coupled ferromagnetic Kondo lattice, we argue that the localized electrons develop magnetic order. Thus, in our picture, the magnetic moment of the system is due primarily to localized electrons.

Our picture for superconductivity is the following. We suppose that there are droplets of local superconductivity in the STO substrate. If the STO were doped, then these droplets would grow and percolate across the system, giving rise to superconductivity. In the absence of doping, this cannot occur, and the STO substrate is insulating. However, these droplets can interact with the itinerant electrons at the interface. Through the proximity effect, superconducting droplets in the STO substrate can induce a gap in the itinerant electrons at the interface. Thus seeded, the itinerant electrons at the interface can develop long-ranged or quasi-long-ranged superconducting order. However, these itinerant electrons must move in the magnetic background created by the localized electrons. Naively, the magnetism should destroy the superconductivity. However, the strong spin-orbit coupling of the interface electrons allows these two competing phenomena to coexist peacefully¹⁸. Spin-orbit coupling mixes s -wave and p -wave superconductivity, so that the s -wave superconductivity which is present in the droplets in STO can induce a mixture of s -wave and p -wave superconductivity at the interface. This mixture can tolerate a magnetic moment, unlike pure s -wave superconductivity. This is very similar to the situation in proposals of topological insulators in contact with s -wave superconductors^{19–21}, superconductor-semiconductor heterostructures^{22,23}, and spin-orbit-coupled quantum wires^{24,25}. Therefore, according to our theory, even though superconductivity is s -wave in STO, interfacial superconductivity is unconventional, as a result of magnetism and spin-orbit coupling.

An especially exciting consequence of the unconventional nature of the interfacial superconductivity is the possibility of

realizing Majorana fermion physics. Indeed, the fabrication of narrow quasi-one dimensional conducting channels on an otherwise insulating LAO/STO interface^{26–28} by ‘writing’ them with an atomic-force microscope (AFM) tip suggests a natural implementation for the proposals of Refs. 24 and 25. In the following sections we show that our model naturally generates a ‘helical’ interfacial band structure that can be driven into a topological phase when in proximity to ordinary s -wave superconductivity. As shown by Kitaev [29], 1D spinless superconductor with p -wave (or effectively p -wave) pairing supports Majorana zero-energy modes at the ends. Although our droplet model can at best lead to quasi-long ranged superconducting order, signatures of Majorana physics still remain, as shown in Refs. [30–32].

In Section II, we set up and justify a model of spin-orbit-coupled itinerant electrons interacting with Kondo spins. In Section III, we give a saddle-point analysis of a large- N limit of this model. In Section IV, we solve this model numerically by the density-matrix renormalization group (DMRG) in the one-dimensional limit. In Section V, we analyze the superconducting proximity effect in the presence of a helical wire due to the presence of ferromagnetic Kondo interactions and spin-orbit coupling. We show that such an interfacial superconducting state might support Majorana zero-energy modes. We conclude in Sec. VI with the discussion of our results and proposing a schematic phase diagram for LAO/STO interface.

II. SPIN-ORBIT-COUPLED FERROMAGNETIC KONDO MODEL

We will now argue for a model of spin-orbit coupled electrons interacting with localized spins to describe the LAO/STO interface. The emerging consensus is that the electrons active at the LAO/STO interface come from the t_{2g} bands of Ti $3d$ orbitals in the STO^{3,10,16,33–38}. Furthermore, band structure calculations³³ and density functional theory³⁶ suggest a picture of successive Ti $3d$ sub-bands near the interface being occupied as LAO thickness is increased (or gate voltage decreased).

Due to the inversion symmetry breaking at the interface, the lowest sub-band is predicted to be d_{xy} . It contains most of the charge required by the polarization catastrophe, but these electrons are thought to be localized, as seen from the low mobile carrier densities extracted from Hall transport measurements. We thus model these electrons as localized spins. Further indirect evidence for a picture involving localized spins in LAO/STO comes from transport experiments on a related system consisting of pure STO, with the doping effect of the LAO simulated by an polarized gel overlayer³⁹. The longitudinal resistance in this system exhibits a Kondo minimum as a function of temperature, indicative of the presence of localized impurity spins.

The lowest extended interface states are thought to have d_{xz} and d_{yz} symmetry. Due to the geometry of their orbitals, their Fermi surfaces are highly anisotropic, with heavy and light carrier directions. Spin-orbit coupling also plays an important role in determining the electronic band-structure, with the au-

thors of Ref. 33 arguing for an atomic spin orbit (ASO) effect of about 10meV. Furthermore, there is a Rashba contribution arising from the broken inversion symmetry of the interface and gating. Its magnitude is expected to be dependent on the gate voltage and the details of the sample, but in Ref. 11 a value of $\alpha \approx 10 - 50 \text{ meV\AA}$ is obtained through a fit to a weak anti-localization measurement. (Larger values close to 50 meV\AA are obtained for larger gate voltages; smaller values, for smaller gate voltages.) The Rashba nature of the coupling was deduced from the dependence of the spin relaxation time on the elastic scattering time. The electronic band-structure for the two dimensional interface depends on the precise ratio of Rashba and ASO coupling.

Motivated by recent experiments fabricating one dimensional conducting channels on otherwise insulating LAO/STO interfaces^{27,28}, as well as by our desire to realize Majorana physics, we find it useful to examine one-dimensional channels at the LAO/STO interface. In a 1D channel, the anisotropy of the d_{xz} , d_{yz} orbitals suggest that for a very narrow channel along the x direction, transport should primarily be through the d_{xz} states¹². Therefore, the neglect of the d_{yz} band is justified in this situation. In Ref. 27 and 28, conducting channels of thickness $\sim 10 \text{ nm}$ are constructed. For an effective mass of order the electron mass, such channels correspond to a transverse confining energy of $\sim 2 \text{ meV}$, and hence in principle we need to consider many subbands at the energy scales in which we are interested. However, if narrower conducting wires could be constructed (e.g. 2 nm , corresponding to $\sim 40 \text{ meV}$), a one dimensional model would be more readily applicable.

We are thus led to analyze a minimal model of a single spinful band interacting with a large density of localized spins. The localized spins, which give the dominant contribution to the magnetic moment come from the d_{xy} band. However, their tendency to order is driven primarily by their interaction with d_{xz} , d_{yz} electrons. Although the experiment of Ref. 39 suggests an antiferromagnetic coupling between conduction and impurity spins, we believe that it is more natural, according to Hund's rule, take the interaction between d_{xy} electrons and d_{xz} , d_{yz} electrons to be ferromagnetic. In either case, the Hamiltonian takes the form

$$H = \sum_{k_x, \lambda, \lambda'} \left[\varepsilon(k_x) \delta_{\lambda, \lambda'} c_{k_x, \lambda}^\dagger c_{k_x, \lambda} + \alpha k_x \sigma_{\lambda, \lambda'}^y c_{k_x, \lambda}^\dagger c_{k_x, \lambda'} \right] + J \sum_{k_x, q, \lambda, \lambda'} c_{k_x+q, \lambda}^\dagger \vec{\sigma}_{\lambda, \lambda'} c_{k_x, \lambda'} \cdot \vec{S}(q) \quad (1)$$

where σ_i is the Pauli matrix acting on a spin degree of freedom, \vec{S} corresponds to classical spins due to localized magnetic impurities, and we have suppressed spin indices in the notation. In a lattice version of this Hamiltonian the kinetic term is modeled by a nearest neighbor hopping t , whose magnitude is determined by band structure calculations^{16,35} to be about 0.2 eV . From magnetoconductance experiments^{11,12} we take $\alpha \approx 10 - 50 \text{ meV\AA}$, which translates to a lattice spin orbit coupling $\alpha a^{-1} \sim t/20$ or even as large as $t/4$ (see below). The final term is the interaction between the itinerant electrons and localized spins. Although we believe that it is

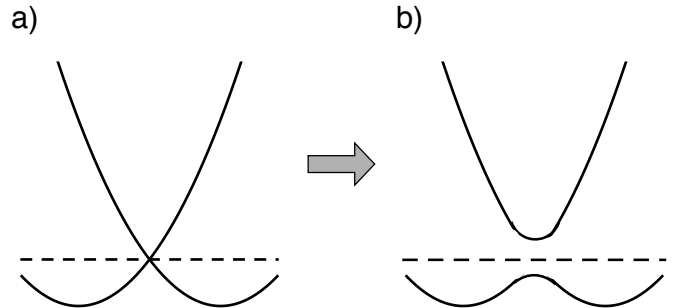


FIG. 1. (a) Sample one dimensional electronic band-structure. We expect a magnetic instability at ordering wave-vector $q = 0$, where a gap can open in the spectrum at the crossing point between the two bands. When this occurs, the band structure takes the form in (b)

more natural, according to Hund's rule, to have a ferromagnetic coupling, $J < 0$, we will also, for completeness, consider the case of antiferromagnetic coupling, $J > 0$, with a magnitude of roughly one third of the bandwidth, as obtained in Ref. 39.

Motivated by recent SQUID⁵ and torque magnetometry⁴ experiments, which find at least local ferromagnetism, we are interested in examining the magnetic instabilities of the Hamiltonian (2). The one dimensional spin-orbit coupled electronic band-structure in figure 1 shows that it is natural to expect ordering at wave-vector $q = 0$, since it is there that a gap can be opened and the electronic energy lowered. Of course, ordering could also occur at the wavevectors that connect various pairs of Fermi points. In the next section we will study a large- N limit of this model and find a tendency toward in-plane ferromagnetism, consistent with [4 and 5]. In the following section we will reach a similar conclusion with DMRG.

III. LARGE- N ANALYSIS OF THE MODEL

We now analyze magnetic instabilities of a generalization of the Hamiltonian (2) to N species of fermions $c_{k_x}^a$, with $a = 1, 2, \dots, N$:

$$H = \sum_{k_x, \lambda, \lambda', a} \left[\varepsilon(k_x) c_{k_x, \lambda}^{a\dagger} c_{k_x, \lambda}^a \delta_{\lambda, \lambda'} + \alpha k_x \sigma_{\lambda, \lambda'}^y c_{k_x, \lambda}^{a\dagger} c_{k_x, \lambda'}^a \right] + J \sum_{k_x, q, \lambda, \lambda'} c_{k_x+q, \lambda}^{a\dagger} \vec{\sigma}_{\lambda, \lambda'} c_{k_x, \lambda'}^a \cdot \vec{S}_q = \sum_{k_x, \lambda, \lambda', a} c_{k_x, \lambda}^{a\dagger} M(k_x, \vec{S})_{\lambda \lambda'} c_{k_x, \lambda'}^a \quad (2)$$

where the matrix $M(k_x, \vec{S})$ is given by

$$M(k_x, \vec{S}) = \begin{bmatrix} \varepsilon(k_x) + JS_z & i\alpha k_x + J(S_x + iS_y) \\ -i\alpha k_x + J(S_x - iS_y) & \varepsilon(k_x) - JS_z \end{bmatrix}. \quad (3)$$

We now integrate out fermions in Eq.(2):

$$\begin{aligned} \exp\left(-S_{\text{eff}}[\vec{S}]\right) &= \int Dc dc^\dagger e^{-S_0[\vec{S}] - \int d\tau \sum_k (c_{k_x}^{a\dagger} i\partial_\tau c_{k_x}^a - H)} \\ &= e^{-S_0[\vec{S}] - N \text{tr} \ln(i\omega_n - M(k_x, \vec{S}))} \end{aligned} \quad (4)$$

where $S_0[\vec{S}]$ is the Berry phase term for the localized spins. In the large- N limit, the functional integral

$$Z[\vec{S}] = \int DS \exp\left(-S_0[\vec{S}] - N \text{tr} \ln\left[i\omega_n - M(k_x, \vec{S})\right]\right) \quad (5)$$

is equal to its saddle-point value. The saddle-point equations are given by:

$$\frac{\partial}{\partial \vec{S}} \left(S_0[\vec{S}] - N \text{tr} \ln\left[i\omega_n - M(k_x, \vec{S})\right] \right) = 0. \quad (6)$$

The $S_0[\vec{S}]$ term is $O(1)$ and is much smaller than the second term which is $O(N)$, so it can be neglected. Since the temperature of interest is much lower than the energy scales associated with the couplings in (2), we can effectively set it to zero and convert Matsubara sum to an integral. Thus, we arrive at the following mean-field equations:

$$\frac{\partial}{\partial \vec{S}} \int \frac{d\omega}{2\pi} \frac{dk_x}{2\pi} \log[(i\omega - E^+(k_x))(i\omega - E^-(k_x, \vec{S}))] = 0, \quad (7)$$

where $E^\pm(k_x)$ are the two eigenvalues of $M(k_x, \vec{S})$:

$$E^\pm(k_x, \vec{S}) = \varepsilon(k_x) \pm Q(k_x, \vec{S}) \quad (8)$$

$$Q(k_x, \vec{S}) = \sqrt{J^2 S_z^2 + J^2 S_x^2 + (\alpha k_x + JS_y)^2} \quad (9)$$

The explicit evaluation of derivatives yields

$$\int \frac{d\omega}{2\pi} \frac{dk_x}{2\pi} \frac{\partial Q(k_x, \vec{S})}{\partial \vec{S}} \left[\frac{1}{i\omega - E^+(k_x, \vec{S})} - \frac{1}{i\omega - E^-(k_x, \vec{S})} \right] = 0. \quad (10)$$

One can notice that we only obtain a non-zero contribution if $E^+(k_x, \vec{S})$ and $E^-(k_x, \vec{S})$ have opposing signs, so that the saddle point equation reduces to

$$\int \frac{dk_x}{2\pi} \left[\Theta(-E^+(k_x, \vec{S})) - \Theta(-E^-(k_x, \vec{S})) \right] \frac{\partial Q(k_x, \vec{S})}{\partial \vec{S}} = 0. \quad (11)$$

Here $\Theta(x)$ is the unit step function ($\Theta(x) = 1$ for $x > 0$) and

$$\frac{\partial Q(k_x, \vec{S})}{\partial \vec{S}} = \frac{J}{Q(k_x, \vec{S})} \begin{pmatrix} JS_x \\ \alpha k_x + JS_y \\ JS_z \end{pmatrix} \quad (12)$$

The \vec{S} -dependent contribution to the energy of a particular background spin configuration at one loop reads

$$E \propto \int \frac{dk}{2\pi} (E_k^+ \Theta(-E_k^+) + E_k^- \Theta(-E_k^-)) \quad (13)$$

To diagonalize, we take nearest neighbor hopping with amplitude normalized to 1, resulting in a kinetic term

$$\varepsilon(k_x) = \cos(k_x) - \mu \quad (14)$$

For convenience we also absorb \vec{S} into J : $\vec{J} \equiv J\vec{S}$, and drop it from the following discussion. We then compute the one loop energy as a function of \vec{J} , μ , and α , and determine the propensity for magnetic ordering in various directions. From (8) we see that the x and z directions become equivalent at one loop, so it suffices to set $J_x = 0$ and work with nonzero J_y and J_z . Symmetry considerations show that $\vec{J} = 0$ is an extremum of the one loop energy. In fact, we empirically see that it is a global maximum, and that the energy is unbounded from below, becoming more negative with increasing $|J|$. This makes sense since the saddle-point Hamiltonian treats \vec{S} as a classical field with no dynamics, and larger $|\vec{S}|$ leads to lower electronic energy. Physically, we expect that $|\vec{S}|$ ultimately saturates. For the purposes of the saddle-point approximation we pick an appropriate value for $|\vec{J}|$ and evaluate the energy difference between ordering in the y and z directions:

$$\begin{aligned} \delta E(\alpha, \mu) &= E(J, 0, \alpha, \mu) - E(0, J, \alpha, \mu) \\ &\approx J^2 (c_z(\alpha, \mu) - c_x(\alpha, \mu)) \end{aligned} \quad (15)$$

In figure 2 we plot $\delta E/|E|$ at a specific value of J , and note that it is everywhere negative. Although the percentage difference in energies is small, it is robustly negative over a very large range of physical values of μ , α , and J . We conclude that in saddle-point approximation the spins prefer to develop magnetic order in the (in-plane) y direction.

We can perform a similar analysis for a two dimensional version of (2), obtaining a similar result: the spins prefer to order in-plane in the large- N limit.

One very interesting part of our analysis is that we find ferromagnetic order developing at *weak coupling*. The underlying reason for this is that the band structure in the presence of Rashba spin-orbit coupling has a crossing at $k = 0$; a small magnetic moment opens a gap there. This occurs even at arbitrarily weak coupling, if the chemical potential passes through this crossing. This is very similar to the case of other Fermi surface instabilities, such as the BCS instability or density-wave ordering for nested Fermi surfaces. If the chemical potential does not pass through the $k = 0$ crossing, then a small minimum coupling must be exceeded, as in the case of small detuning away from a nested Fermi surface. This scenario stands in stark contrast to the usual case of the Stoner instability: ordinarily, ferromagnetism does not open a gap at the Fermi surface, and only occurs when the coupling exceeds the inverse of the density of states.

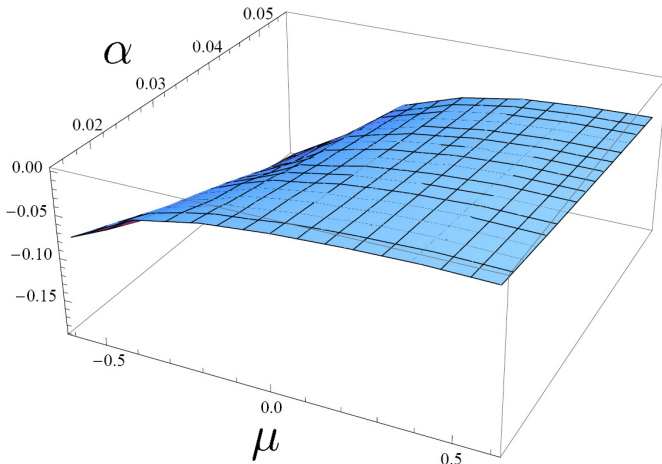


FIG. 2. $-(\delta E)/|E|$, where δE is defined in (15), plotted at $J = 0.4$ as a function of chemical potential μ and spin-orbit coupling α for a one dimensional conducting wire aligned in the y direction sitting on the 2 dimensional xy plane. We note that this quantity is everywhere negative, implying a propensity towards magnetic ordering in plane, perpendicular to the wire *i.e.* along the x direction. Other values of J give similar results.

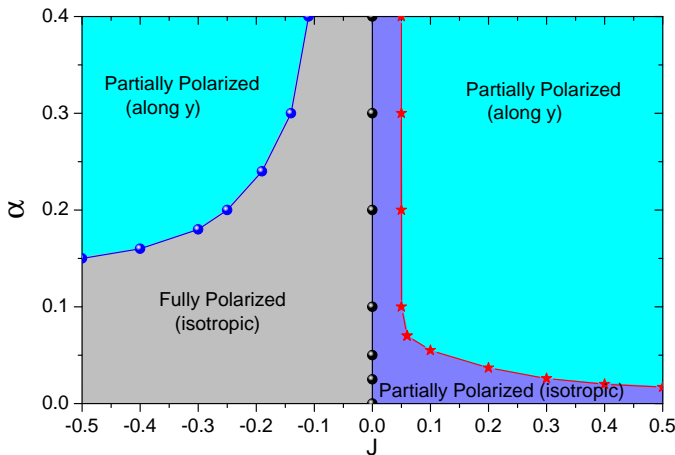


FIG. 3. (color online) Ground state phase diagram of the model Hamiltonian in Eq.(16) at filling $\rho = 1/6$, determined by accurate DMRG simulations with system size up to $N = 192$ sites. Changing coupling parameters J and αa^{-1} , three different phases are found, including the fully polarized phase, the partially polarized phase, as well as the easy-plane partially polarized phase. Here $J_{\text{chain}} = 0.1t$ and $U = 40t$.

IV. DMRG SOLUTION OF THE 1D LIMIT

We now consider a 1D lattice Hamiltonian describing itinerant electrons coupled to localized impurity spins:

$$\begin{aligned}
 H = & -t \sum_{i,\alpha} (c_{i\alpha}^\dagger c_{i+1\alpha} + h.c.) + J \sum_{i,\alpha,\beta} \vec{S}_i \cdot c_{i\alpha}^\dagger \vec{\sigma}_{\alpha\beta} c_{i\beta} \\
 & - J_{\text{chain}} \sum_i \vec{S}_i \cdot \vec{S}_{i+1} \\
 & + \frac{\alpha}{a} \sum_i (c_{i\uparrow}^\dagger c_{i+1\downarrow} - c_{i\downarrow}^\dagger c_{i+1\uparrow} + h.c.) \\
 & + U \sum_i n_{i\uparrow} n_{i\downarrow} - h_z \sum_i (S_i^z + \tau_i^z) - h_y \sum_i (S_i^y + \tau_i^y).
 \end{aligned} \tag{16}$$

Here $c_{i\alpha}^\dagger$ ($c_{i\alpha}$) is the electron creation (annihilation) operator with spin index $\alpha = (\uparrow, \downarrow)$ at site i ; \vec{S}_i is the $S = \frac{1}{2}$ spin operator, representing the localized magnetic moment; t denotes the nearest neighbor (NN) tunneling matrix element (henceforth we set $t = 1$) and a is the lattice constant. J is the Kondo coupling between localized magnetic moments and itinerant electrons, J_{chain} is the ferromagnetic exchange coupling between NN localized magnetic moments, and α is the spin-orbit coupling. U is the on-site Hubbard repulsion for the itinerant electrons, and we have also included Zeeman terms for both the localized spin and itinerant electron spin along the z and y directions. In the Hamiltonian (16), impurity spins have their own dynamics and the ground-state of the is determined by taking into account both electron and spin degrees of freedom on equal footing. If we use mean-field approximation for impurity spins, *i.e.* $\langle \vec{S}_i \rangle = \vec{S}(x_i)$, and neglect electron-electron interaction, we obtain the Hamiltonian (2) considered in the previous section. As we show below, our conclusions regarding preferred magnetization persist in the strongly interacting limit $U \gg t$.

In our picture, most of the electrons required by the polarization catastrophe argument become localized d_{xy} spins, with a much lower density of itinerant electrons. Therefore, we focus on the low density case, taking $\rho = 1/6$ for the sake of concreteness in most of our calculations. The coupling parameters are taken to have values $U = 40t$ and $J_{\text{chain}} = t/10$. (However, our results are not very sensitive to the value of J_{chain} .) We then map out the phase diagram as a function of αa^{-1} and J . By the arguments given in Sec. II, we expect that $\alpha a^{-1} \approx t/40$ and $J \approx -0.3t$. However, given that there is some uncertainty in these parameters, it behooves us at this stage to see how the physics of our Hamiltonian changes as we vary them. We have included small magnetic fields in the y - and z -directions. These fields are necessary to break time-reversal symmetry and rotational symmetry about the S^y -axis; otherwise, we would necessarily find $\langle S^y \rangle = \langle S^z \rangle = 0$. In an infinite system, but in the absence of these symmetry-breaking fields, the system can spontaneously choose to order along S^y or $-S^y$ or it could spontaneously pick a direction in the $S^z - S^x$ plane (if it orders at all). Employing the unbiased density matrix renormalization group⁴⁰ method, we determine the ground-state phase diagram of the system (16).

We find the following phase diagram, depicted in Fig.3. For

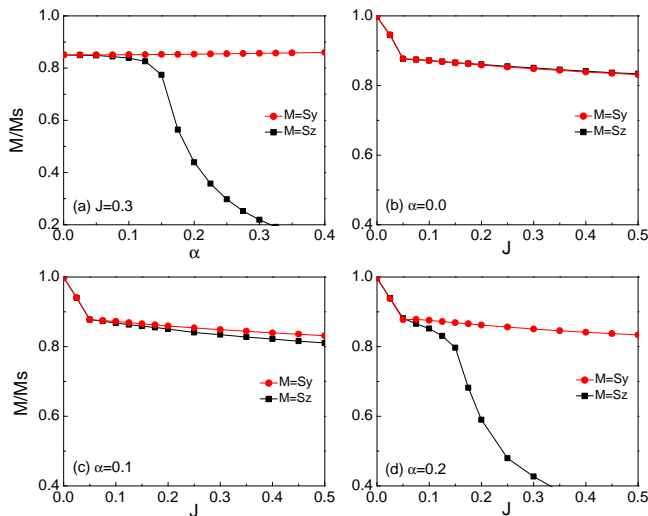


FIG. 4. (color online) Relative polarization M/M_s as functions of αa^{-1} and J , along y direction ($M = S^y$) and z direction ($M = S^z$), for the system in Eq.(16) at filling $\rho = 1/6$ and system size $N = 192$ sites. Relative polarization M/M_s for $J = 0.3$ in (a), $\alpha a^{-1} = 0.0$ in (b), $\alpha a^{-1} = 0.1$ in (c), and $\alpha a^{-1} = 0.2$ in (d). Here $J_{\text{chain}} = 0.1t$, $U = 40t$, and M_s is the saturated magnetization. Note that the polarization is induced by applying a small magnetic field $h_y = 0.005t$ along y direction or $h_z = 0.005t$ along z direction separately.

J large and negative (i.e. a ferromagnetic coupling between localized and itinerant spins) and αa^{-1} large, the system is partially-polarized and the moment points in the y -direction (i.e. in plane, but perpendicular to the nanowire, and corresponding to the light blue region in the upper left corner of Fig.3). For $J < 0$ but lying below the blue phase boundary in Fig. 3, we have a fully-polarized phase in which the spins can point equally-well in any direction (the grey region near the middle of Fig.3). For $J > 0$, there is a partially-polarized phase at small J or small αa^{-1} (narrow purple region). In this region, the spins can point equally-well in any direction. Finally, if J is positive and either J or αa^{-1} is large, then the system is partially-polarized and the spins point in the y -direction (light blue region in upper right of Fig. 3).

We now examine the magnetically-ordered state in more detail. The occupation number $n(k) = \langle c_{\uparrow}^{\dagger} c_{\uparrow} + c_{\downarrow}^{\dagger} c_{\downarrow} \rangle$ clearly shows a filled Fermi sea with approximately one electron in each occupied state, with $|k| < k_F$, as illustrated in Fig. 5a, at the parameter values listed in Fig. 5b. The Fermi wavevector is consistent with $k_F = \pi/3$, in agreement with Luttinger's theorem. The structure factor $\rho(q)\rho(-q)$ shown in Fig. 5b has cusps at $\pm 2k_F$, from which we can more precisely extract the Fermi wavevector $k_F = \pi/3$. The occupation numbers and Luttinger volume are consistent with the chemical potential depicted in Figure 1. There are two Fermi points and there is a single state at each Fermi point because the spin is locked to the momentum. Such a 1D electron gas is often called a ‘‘helical wire’’. (Note that our system is not simply fully spin-polarized; we have checked that, at these parameter values, neither $\langle c_{\uparrow}^{\dagger} c_{\uparrow} \rangle$ nor $\langle c_{\downarrow}^{\dagger} c_{\downarrow} \rangle$ is ever equal to one, so the spins are

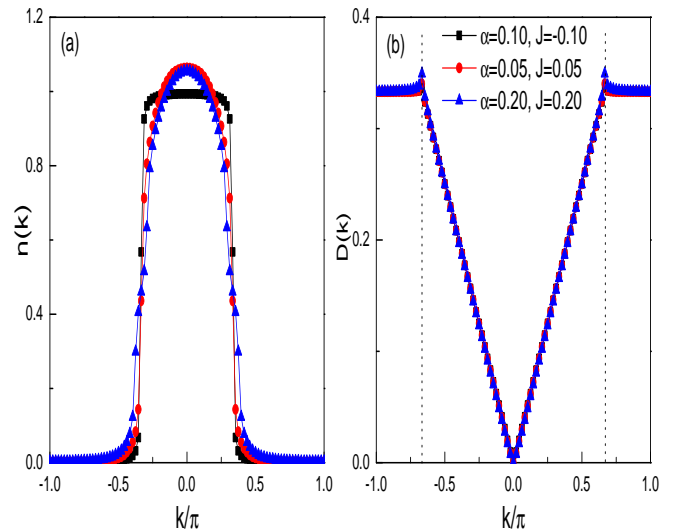


FIG. 5. (color online) The Fermi surface of our 1D model at three points in the phase diagram. (a) The occupation number $n(k) = \langle c_{\uparrow}^{\dagger} c_{\uparrow} + c_{\downarrow}^{\dagger} c_{\downarrow} \rangle$, which shows the region of momentum space occupied by the filled Fermi sea. (b) The equal-time density-density correlation function, which has singularities at $2k_F$.

not polarized in the z -direction; they are also not equal to each other, so the spins are not polarized in the x - or y -directions.) Therefore, an odd number of bands (in fact, just one) crosses the Fermi surface; as we discuss in Section V, this means that the system is primed for the development of topological superconductivity.

V. PROXIMITY-INDUCED SUPERCONDUCTIVITY

We propose the following picture for superconductivity at the LAO/STO interface. Our starting point is superconductivity in STO, which occurs when insulating STO is doped. We assume that insulating STO has small islands or droplets of local superconductivity, which are too far apart and too weakly-coupled to develop long-ranged superconducting order. We suppose that these droplets are caused by unintentional local defects in STO. When STO is doped, the islands of local superconductivity grow in size and become more strongly coupled, until long-ranged superconducting order sets in. However, the presence of an interface with LAO changes matters. Itinerant electrons at the interface can mediate a coupling between superconducting droplets in STO that are close to the interface. As we will show, this can enable superconductivity to develop even when the droplets are too weakly-coupled to percolate across STO on their own.

We show how this can occur with a calculation in a simplified model. We suppose that there are some superconducting droplets in STO that are near the LAO/STO interface. In each droplet, a single-particle gap is assumed to be well-developed, but the interactions between the droplets are assumed to be too weak for superconducting order to set in. A 1D channel at the

interface couples to a subset of these droplets, which form a linear array. The 1D channel induces interactions between the droplets, so that the linear array can be modeled as a 1D spin-gapped electron system, which we assume to be just slightly on the disordered side of the Kosterlitz-Thouless transition. (Since doped STO superconducts, this is a reasonable approximation.) The coupling between this system and a 1D channel at the LAO/STO interface can nudge the system into the basin of attraction of the quasi-long-range ordered superconducting phase on the other side of the Kosterlitz-Thouless transition. We thereby see how proximity to a metallic interface can stabilize long-ranged or quasi-long-ranged superconducting order.

Once superconductivity is established in STO, it is induced at the interface by the proximity effect. This mechanism of establishing superconducting order works for generic conducting 1D channels. However, the interesting scenario for us occurs when, due to Rashba spin-orbit coupling and ferromagnetism, the 1D channel realizes the helical band structure in Fig 1, and the induced superconductivity is topological. Hence, we begin with a bosonized helical 1D channel at the interface, coupled to an array of isolated, *i.e.* effectively zero dimensional, droplets:

$$S = \frac{v_F}{2\pi} K_w \int dx d\tau [(\partial_x \theta)^2 + v_F^{-1} (\partial_\tau \theta)^2] + \frac{1}{2U_j} \sum_j (\partial_\tau \theta_j)^2 + \Delta_{P,j} \sum_j \left(e^{2i\theta(x_j)} e^{-i\sqrt{2}\theta_j} + \text{c.c.} \right) \quad (17)$$

Here, v_F is the Fermi velocity in the 1D channel and K_w is its Luttinger parameter. The 1D channel is assumed to have repulsive interactions, so $K_w < 1$. The factor of $\sqrt{2}$ in the exponent in the third line has been inserted for later convenience so that it agrees with the convention for the charge boson of a spin-gapped electron system (see, for instance, Ref. 30). The droplets are assumed to have an average spacing a , an average Josephson coupling Δ_P to the 1D channel, and an average charging energy U . We will neglect random variations in the spacing between droplets, in the Josephson couplings, and in the charging energies, and simply set $x_j = ja$, $\Delta_{P,j} = \Delta_P$, and $U_j = U$. Random variations in these parameters are certainly important in the physical system but are an unnecessary complication for this calculation. Note that if $\Delta_P = 0$, then the droplets are completely decoupled from each other and there is no quasi-long-ranged superconducting order.

We now integrate out fluctuations of θ at length scales shorter than ℓ . This generates a coupling between droplets. At length scales much longer than ℓ , we can take the continuum limit for the array of droplets, thereby leading to the following effective action:

$$S = \frac{1}{2\pi} \int dx d\tau \left(v_F K_w [(\partial_x \theta)^2 + v_F^{-2} (\partial_\tau \theta)^2] + v K_\rho [(\partial_x \theta_\rho)^2 + v^{-2} (\partial_\tau \theta_\rho)^2] - \frac{\Delta_P}{a} \cos(2\theta - \sqrt{2}\theta_\rho) \right) \quad (18)$$

The droplets are now effectively described by a 1D wire with a spin gap; θ_ρ is the charge boson for such a wire. Since we assume that there is, initially, a weak interaction between the droplets and the 1D channel, we assume that $K_\rho < 1$. In other words, although the wire has a spin gap, we do not assume that it can superconduct without further mediation on the part of the 1D channel at the interface. Indeed, the parameters K_ρ and v can be related to the effective superfluid stiffness ρ_s and compressibility κ of the array: $K_\rho = 2\pi\sqrt{A_w \rho_s \kappa}$ and $v = \sqrt{A_w \rho_s / \kappa}$ with being A_w the cross-sectional area. We assume here that the superfluid stiffness is such that $K_\rho < 1$.

If the two velocities were equal, $v = v_F$, one could analyze the model by forming the combinations $\theta_\pm = (\sqrt{2}\theta_\rho \pm 2\theta)/2$. In terms of new variables θ_\pm the action reads

$$S = \frac{v}{2\pi} \int dx d\tau \left(\left(\frac{K_w}{4} + \frac{K_\rho}{2} \right) [(\partial_\mu \theta_+)^2 + (\partial_\mu \theta_-)^2] - 2 \left(\frac{K_w}{4} - \frac{K_\rho}{2} \right) \partial_\mu \theta_+ \partial_\mu \theta_- - 2y \cos(2\theta_-) \right). \quad (19)$$

Here, we have rescaled the time coordinate by v and have introduced the dimensionless parameter $y = \Delta_P a / 2v$. We can now see, at a heuristic level, how the coupling between the droplets and the 1D channel can stabilize quasi-long-ranged superconducting order. Let us suppose, for a moment, that the coupling y is relevant. Then θ_- is pinned, and we can ignore its fluctuations. Then we are left with θ_+ , which exhibits algebraically-decaying superconducting order. This order is stable if weak impurity-backscattering or, equivalently, vortex tunneling is irrelevant. Because the wire is helical, we can only tunnel $\frac{hc}{e}$ vortices³⁰, *i.e.* $\theta \rightarrow \theta + 2\pi$. Since θ_- is pinned, this means that θ_ρ must also wind $\theta_\rho \rightarrow \theta_\rho + 2\pi\sqrt{2}$. Consequently, in such a process, $\theta_+ \rightarrow \theta_+ + 4\pi$. The operator that accomplishes this is $\sin(4\phi_+)$, where $[\phi_+(x), \partial_x \theta_+(y)] = i\pi\delta(x-y)$. This operator is irrelevant if $2K_\rho + K_w > 1$, and when this inequality is satisfied, the system exhibits quasi-long-ranged superconducting order. Note that this can be satisfied even if $K_\rho < 1$ and $K_w < 1$. So two systems, neither of which could sustain superconductivity on their own, can develop superconductivity when in proximity to each other. The key to this is the topological nature of the superconductivity: since only $\frac{hc}{e}$ vortices can tunnel through a helical wire, the stability condition is less strict than for an ordinary superconductor⁴¹.

To support the aforementioned scenario, we need to show that that Cooper-pair tunneling term is relevant. The corresponding RG equation for y is:

$$\frac{dy}{d\ell} = [2 - (K')^{-1}] y, \quad (20)$$

where $(K')^{-1} \equiv \frac{1}{2K_\rho} + \frac{1}{K_w}$. If $(K')^{-1} < 2$, y will grow from the initial small value $y(0) \ll 1$ to $y(\ell) \sim 1$ at which point θ_- gets pinned. Given that K' also flows under RG, we need to compute its flow equation and complete the system of RG equations for this model. To do that we rewrite Eq. (19)

in the following form:

$$S = \frac{v}{2\pi} \int dx d\tau \left(K_+ (\partial_\mu \theta_+)^2 + K_- (\partial_\mu \theta_-)^2 - 2K_{+-} (\partial_\mu \theta_+ \partial_\mu \theta_-) - 2y \cos(2\theta_-) \right) \quad (21)$$

where, initially, $K_+ = K_- = \frac{K_w}{4} + \frac{K_\rho}{2}$, $K_{+-} = \frac{K_w}{4} - \frac{K_\rho}{2}$. The reason that we have introduced three couplings K_+ , K_- , K_{+-} when there are, seemingly, only two couplings K_w and K_ρ is that the RG flow for this theory will carry the system away from the initial point $K_+ = K_-$. A real-space RG calculation yields the following equations for K_- , K_+ , K_{+-} :

$$\frac{dK_-}{d\ell} = y^2, \quad \frac{dK_+}{d\ell} = \frac{dK_{+-}}{d\ell} = 0. \quad (22)$$

The coupling K' can be expressed in terms of K_- , K_+ and K_{+-} (or equivalently in terms of K_- and the initial parameters K_ρ and K_w since K_{+-} and K_+ do not flow):

$$K' = K_- - K_{+-}^2 / K_+ = K_- - \frac{(2K_\rho - K_w)^2}{4(2K_\rho + K_w)}. \quad (23)$$

Since K' monotonically depends K_- , the growth of K_- under the RG flow results in

$$\frac{dK'}{d\ell} = y^2. \quad (24)$$

Thus, the y -coupling becomes more and more relevant, and eventually pins θ_- as assumed above.

We now consider more general case of unequal velocities $v \neq v_F$. Proceeding as before, we find that Eq. (19) can be written as

$$S = \frac{1}{2\pi} \int dx d\tau \left(\tilde{K} (\tilde{v} (\partial_x \theta_-)^2 + \tilde{v}^{-1} (\partial_\tau \theta_-)^2) + \tilde{K}_+ (\tilde{v}_+ (\partial_x \theta_+)^2 + \tilde{v}_+^{-1} (\partial_\tau \theta_+)^2) - 2\tilde{K}_{+-} (\tilde{v}_{+-} (\partial_x \theta_+) (\partial_x \theta_-) + \tilde{v}_{+-}^{-1} (\partial_\tau \theta_+) (\partial_\tau \theta_-)) - 2y \cos(2\theta_-) \right) \quad (25)$$

where the coupling constants are defined as

$$\tilde{K}_+ = \frac{1}{4\sqrt{vv_F}} \sqrt{(K_w v_F + 2K_\rho v) (K_w v + 2K_\rho v_F)} \quad (26)$$

$$\tilde{v}_+ = \sqrt{vv_F \frac{2K_\rho v + K_w v_F}{2K_\rho v_F + K_w v}} \quad (27)$$

$$\tilde{K}_{+-} = \frac{1}{4\sqrt{vv_F}} \sqrt{(K_w v_F - 2K_\rho v) (K_w v - 2K_\rho v_F)} \quad (28)$$

$$\tilde{v}_{+-} = \sqrt{vv_F \frac{K_w v_F - 2K_\rho v}{K_w v - 2K_\rho v_F}} \quad (29)$$

The parameters \tilde{K} and \tilde{v} are initially equal to \tilde{K}_+ and \tilde{v}_+ , respectively, but they flow under RG as explained above.

We now sketch the real-space RG procedure. We start out by integrating out short-distance modes, but allowing arbitrarily short times. Thus, we have an effective action in which there are modes $\theta(k, \omega)$ with $|k| < a^{-1}$ and $|\omega| < \infty$, where a^{-1} is the momentum cutoff. Following a real-space RG approach⁴¹, we integrate shells $a < r < as$ while keeping time integrals unconstrained and eventually rescale $r \rightarrow sr$, $\tau \rightarrow s\tau$. Here $s = e^{d\ell}$. Our RG procedure involves calculating the correlation function $\langle e^{2i\theta_-(x_1, \tau_1)} \cdot e^{-2i\theta_-(x_2, \tau_2)} \rangle$. To do it safely one has to normal order the exponent:

$$e^{2i\theta_-(1)} \cdot e^{-2i\theta_-(2)} =: e^{2i[\theta_-(1) - \theta_-(2)]} : e^{-2\langle [\theta_-(1) - \theta_-(2)]^2 \rangle} \quad (30)$$

where $\theta(1) \equiv \theta(x_1, \tau_1)$, and the average $\langle \dots \rangle$ is computed with respect to the bare action ($y = 0$) defined in Eq. (25). Initially, when $\tilde{K} = \tilde{K}_+$ and $\tilde{v} = \tilde{v}_+$, the correlation function in Eq. 30 can be easily calculated

$$e^{-2\langle [\theta_-(x, \tau) - \theta_-(0, 0)]^2 \rangle} = \frac{a^{\frac{1}{2K_\rho} + \frac{1}{K_w}}}{(x^2 + v^2 \tau^2)^{\frac{1}{2K_\rho}} (x^2 + v_F^2 \tau^2)^{\frac{1}{K_w}}}. \quad (31)$$

However, in general it is a complicated function of the coupling constants (26) as well as \tilde{K} and \tilde{v} . One can show that at the tree-level the RG equation for y becomes

$$\frac{dy}{d\ell} = [2 - (K')^{-1}] y \quad (32)$$

where, again, $(K')^{-1} \equiv \frac{1}{2K_\rho} + \frac{1}{K_w}$.

We now compute the RG equations for this model at one-loop level. Using Eqs.(30) and (31), we find

$$\frac{d}{d\ell} (\tilde{K} \tilde{v}) = \sqrt{vv_F} f_2 \left(\frac{v_F}{v} \right) y^2, \quad (33)$$

$$\frac{d}{d\ell} (\tilde{K} \tilde{v}^{-1}) = \frac{1}{\sqrt{vv_F}} f_0 \left(\frac{v_F}{v} \right) y^2, \quad (34)$$

where $y = \Delta_P a / \sqrt{vv_F}$ and the dimensionless function

$$f_n(\kappa) = \frac{1}{8\pi} \int_{-\infty}^{\infty} dz \frac{z^n}{(\kappa^{-1} + z^2)^{\frac{1}{2K_\rho}} (\kappa + z^2)^{\frac{1}{K_w}}}. \quad (35)$$

As follows from Eqs.(33), the RG equations for \tilde{K} and \tilde{v} are given by

$$\frac{d\tilde{K}}{d\ell} = \frac{y^2}{2} \left[\frac{\tilde{v}}{\sqrt{vv_F}} f_0 \left(\frac{v_F}{v} \right) + \frac{\sqrt{vv_F}}{\tilde{v}} f_2 \left(\frac{v_F}{v} \right) \right] \quad (36)$$

$$\frac{d\tilde{v}}{d\ell} = \frac{1}{2\tilde{K}} \left[\sqrt{vv_F} f_2 \left(\frac{v_F}{v} \right) - \frac{\tilde{v}^2}{\sqrt{vv_F}} f_0 \left(\frac{v_F}{v} \right) \right]. \quad (37)$$

Thus, according to these Kosterlitz-Thouless-type RG equations, Eqs. (32),(36) and 37, we see that \tilde{K} grows. The parameter K' has a complicated dependence on \tilde{K} and \tilde{v} which

VI. DISCUSSION

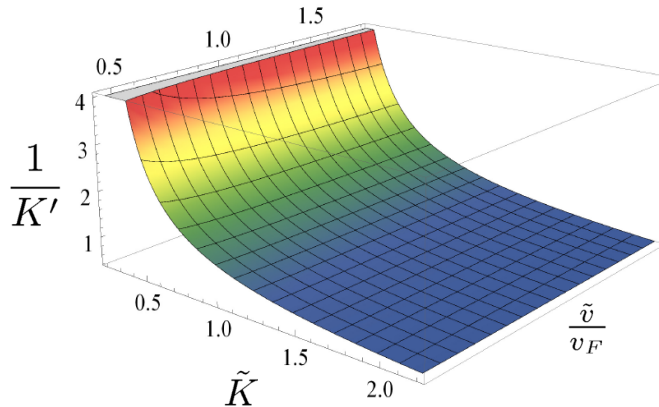


FIG. 6. Dependence of K' on the flow parameters \tilde{K} and \tilde{v} . Here we used $K_w = 0.8$, $K_\rho = 0.2$ and $v = 0.5v_F$. The function K' is a monotonically increasing function of \tilde{K} .

follows from Eq. (31). However, at small initial velocity mismatch $|\delta v| \equiv |v - v_F| \ll v_F$, one finds

$$(K')^{-1} \approx \left[\tilde{K} - \frac{(2K_\rho - K_w)^2}{4(2K_\rho + K_w)} \right]^{-1} - \frac{32\tilde{K}(K_w^2 - 4K_\rho^2)K_\rho(3K_w + 2K_\rho)}{[4(2K_\rho + K_w)\tilde{K} - (2K_\rho - K_w)^2]^3} \frac{\delta v^2}{v_F^2} \quad (38)$$

One can see that the δv^2 -correction is quickly decaying with \tilde{K} and thus do not change qualitatively our results obtained for the $v = v_F$ case, cf. with Eq. (23). In general, we find that K' is a monotonically increasing function of \tilde{K} , see Fig. 6. Thus, the growth of \tilde{K} implies the growth of K' . Therefore, once relevant, y will grow to strong coupling $y(l^*) \sim 1$ and pin θ_- . In this case, θ_- drops out from Eq. (25) and the effective action now reads:

$$S = \frac{1}{2\pi} \int dx d\tau \tilde{K}(l^*) \left(\tilde{v}(l^*) (\partial_x \theta_+)^2 + \tilde{v}(l^*)^{-1} (\partial_\tau \theta_+)^2 \right). \quad (39)$$

Following the argument that we used for $v = v_F$, we observe that quasi-long-ranged order is stable so long as flux hc/e vortex tunneling is irrelevant, i.e. when $\sin(4\phi_+)$ is irrelevant. This occurs when $4\tilde{K} > 1$. Note that this can be satisfied even if $K_\rho < 1$ and $K_w < 1$. As in the equal velocity case, two systems, neither of which could sustain superconductivity on their own, can develop superconduct when in proximity as a result of the helical nature of one of the systems.

We thereby arrive at the model of Ref. 30: a 1D channel that is proximity-coupled to a quasi-long-range-order superconducting wire. As shown there, such a wire supports Majorana zero modes. We also expect our results discussed in this section to apply to multichannel nanowires with an odd number of occupied subbands coupled to superconducting droplets, see, e.g., Refs. 42–44.

In this paper, we have adopted the point of view that SrTiO₃ has the seeds of both magnetism and superconductivity. However, these local tendencies only come to fruition when brought into contact with a metallic layer or 1D channel. We have focussed on the latter case, for reasons of tractability as well as potential relevance to the experiments of Refs. 27 and 28, but we believe that our general mechanism works in 2D as well. We have shown that local moments in SrTiO₃ that are near the LAO/STO interface can order ferromagnetically, as a result of their interaction with mobile electrons at the interface. We have also shown that droplets of local superconductivity in STO – which would interact too weakly to develop superconducting order if left to their own devices – can develop superconducting order as a result of their interaction with mobile electrons at the interface. Finally, we have noted that the interface electrons can form a topological superconducting state as a result of their proximity to ferromagnetic and superconducting order.

We have shown that our model leads to ferromagnetism by two different calculations: a large- N calculation and a DMRG calculation. Both calculations find a ferromagnetic state with spins pointing in the plane, *i.e.* along y -axis with x being the direction along the wire. (In the DMRG calculation, the polarization may be either partial or full, depending on the strength of the spin-orbit coupling.) Interestingly, our large- N calculation finds a ferromagnetic state even at weak coupling, which is a feature of the band structure in the presence of Rashba spin-orbit coupling. A 1D wire with sufficiently strong spin-orbit coupling and Zeeman field will form a helical wire. Our calculations – both large- N and DMRG – show that our model gives rise to a helical wire. Remarkably, recent transport measurements can be interpreted as evidence that 1D channels at the LAO/STO interface are helical wires⁴⁵.

In a helical wire, it is possible for s -wave superconductivity to coexist with a magnetic moment. As a result our model allows for a proximity coupling between s -wave superconducting droplets in STO and ferromagnetic electrons at the LAO/STO interface. We have analyzed our model for superconductivity by mapping it to the theory of a single 1D boson in the vicinity of the Kosterlitz-Thouless transition. We find that such a model could be on the disordered side of the Kosterlitz-Thouless transition for very weak coupling between the droplets and a 1D channel at the interface but it could be on the ordered side of the transition if the coupling is sufficiently strong.

Our results on magnetism and superconductivity imply that the superconducting state of a 1D channel at the LAO/STO interface is in a topological superconducting state. This actually stabilizes the system against quantum phase slips: 2π phase slips are forbidden, and only 4π phase slips, which are less relevant in the RG sense, could disrupt the superconductivity. Furthermore, this topological superconducting state supports Majorana fermion zero modes, whose presence would lead to a 4π -periodic ac Josephson effect^{24,29}.

The main goal of our work has been to show why magnetism occurs, why superconductivity occurs, and why they

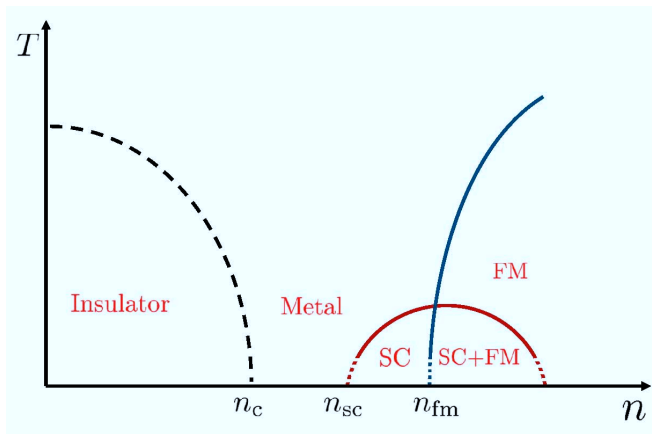


FIG. 7. A schematic phase diagram for the LAO/STO interface as a function of carrier concentration.

can coexist. However, magnetism is probably not found at all carrier concentrations above the metal-insulator transition⁴⁶. Neither is superconductivity. A plausible schematic phase diagram is given in Fig. 7, based on the phase diagram in Refs. 47 and 48. Therefore, it is also important to understand when and why they do not occur. If the magnetic order is too strong, so that the spins are fully polarized, then our mechanism does not work. This may explain why superconductivity is suppressed at large carrier concentration. However, a more detailed understanding of the phase diagram is definitely an im-

portant target for further investigation.

We note that our calculations rely heavily on simplifying features of one dimensional systems – the applicability of DMRG calculations to the magnetic ordering of the system and the applicability of bosonization to the superconducting ordering of the system. It would be interesting to give a fully two-dimensional analysis of a model similar to ours. Furthermore, it would be useful to investigate other related materials exhibiting the same phenomena. In particular, recent work on epitaxially grown GdTiO₃-SrTiO₃ interfaces⁴⁷ indicates that ferromagnetism and superconductivity can also coexist in such systems. Being much cleaner than LAO/STO from a materials point of view, these interfaces might provide an attractive environment for the investigation of the ideas proposed in this paper.

ACKNOWLEDGMENTS

We would like to thank Guanglei Cheng, Harold Hwang, Jeremy Levy, Susanne Stemmer, and Joshua Veazey for discussions. H.C.J. is partially supported by the the KITP NSF grant PHY05-51164 and the NSF MRSEC Program under Award No. DMR 1121053. C.N. is supported by the DARPA QuEST program and the AFOSR under grant FA9550-10-1-0524. We thank the Aspen Center for Physics for hospitality and support under NSF grant #1066293.

- ¹ A. Ohtomo and H. Y. Hwang, *Nature (London)* **427**, 423 (2004).
- ² A. Brinkman, M. Huijben, M. van Zalk, J. Huijben, U. Zeitler, J. C. Maan, W. G. van der Wiel, G. Rijnders, D. H. A. Blank, and J. W. M. Hilgenkamp, *Nature Materials* **6**, 493 (2007).
- ³ Ariando, X. Wang, G. Baskaran, Z. Q. Liu, J. Huijben, J. B. Yi, A. Annadi, A. R. Barman, A. Rusydi, S. Dhar, Y. P. Feng, J. Ding, H. Hilgenkamp, and T. Venkatesan, *Nature Communications* **2** (2011).
- ⁴ L. Li, C. Richter, J. Mannhart, and R. C. Ashoori, *Nature Physics* **7**, 762 (2011).
- ⁵ J. A. Bert, B. Kalisky, C. Bell, M. Kim, Y. Hikita, H. Y. Hwang, and K. A. Moler, *Nature Physics* **7**, 767 (2011).
- ⁶ N. Reyren, S. Thiel, A. D. Caviglia, L. F. Kourkoutis, G. Hammerl, C. Richter, C. W. Schneider, T. Kopp, A.-S. Ruetschi, D. Jaccard, M. Gabay, D. A. Muller, J.-M. Triscone, and J. Mannhart, *Science* **317**, 1196 (2007).
- ⁷ J. Mannhart and D. G. Schlom, *Science* **327**, 1607 (2010).
- ⁸ P. Fulde and R. A. Ferrell, *Physical Review* **135**, A550 (1964).
- ⁹ A. I. Larkin and Y. N. Ovchinnikov, *Sov. Phys. JETP* **20**, 762 (1965).
- ¹⁰ R. Pentcheva and W. E. Pickett, *Phys. Rev. B* **74**, 035112 (2006).
- ¹¹ A. D. Caviglia, M. Gabay, S. Gariglio, N. Reyren, C. Cancellieri, and J.-M. Triscone, *Phys. Rev. Lett.* **104**, 126803 (2010).
- ¹² A. Fête, S. Gariglio, A. D. Caviglia, J.-M. Triscone, and M. Gabay, arXiv:1203.5239 (2012).
- ¹³ M. Ben Shalom, M. Sachs, D. Rakhmilevitch, A. Palevski, and Y. Dagan, *Phys. Rev. Lett.* **104**, 126802 (2010).
- ¹⁴ D. A. Dikin, M. Mehta, C. W. Bark, C. M. Folkman, C. B. Eom, and V. Chandrasekhar, *Physical Review Letters* **107**, 056802+ (2011).
- ¹⁵ K. Michaeli, A. C. Potter, and P. A. Lee, *Phys. Rev. Lett.* **108**, 117003 (2012).
- ¹⁶ Z. S. Popovic, S. Satpathy, and R. M. Martin, *Phys. Rev. Lett.* **101**, 256801 (2008).
- ¹⁷ S. Okamoto and A. J. Millis, *Nature (London)* **428**, 630 (2004).
- ¹⁸ L. P. Gor'kov and E. I. Rashba, *Phys. Rev. Lett.* **87**, 037004 (2001).
- ¹⁹ L. Fu and C. L. Kane, *Phys. Rev. Lett.* **100**, 096407 (2008).
- ²⁰ L. Fu and C. L. Kane, *Phys. Rev. B* **79**, 161408 (2009).
- ²¹ A. Cook and M. Franz, *Phys. Rev. B* **84**, 201105 (2011).
- ²² J. D. Sau, R. M. Lutchyn, S. Tewari, and S. Das Sarma, *Phys. Rev. Lett.* **104**, 040502 (2010).
- ²³ J. Alicea, *Phys. Rev. B* **81**, 125318 (2010).
- ²⁴ R. M. Lutchyn, J. D. Sau, and S. Das Sarma, *Phys. Rev. Lett.* **105**, 077001 (2010).
- ²⁵ Y. Oreg, G. Refael, and F. von Oppen, *Phys. Rev. Lett.* **105**, 177002 (2010).
- ²⁶ C. Cen, S. Thiel, G. Hammerl, C. W. Schneider, K. E. Andersen, C. S. Hellberg, J. Mannhart, and J. Levy, *Nature Materials* **7**, 298 (2008).
- ²⁷ C. Cen, D. F. Bogorin, C. Wung Bark, C. M. Folkman, C.-B. Eom, and J. Levy, arXiv:1009.2424 (2010).
- ²⁸ F. Bi, D. F. Bogorin, C. Cen, C. W. Bark, J.-W. Park, C.-B. Eom, and J. Levy, *Applied Physics Letters* **97** (2010).
- ²⁹ A. Y. Kitaev, *Physics-Uspekhi* **44**, 131 (2001).

- ³⁰ L. Fidkowski, R. M. Lutchyn, C. Nayak, and M. P. A. Fisher, *Phys. Rev. B* **84**, 195436 (2011).
- ³¹ J. D. Sau, B. I. Halperin, K. Flensberg, and S. Das Sarma, *Phys. Rev. B* **84**, 144509 (2011).
- ³² M. Cheng and H.-H. Tu, *Phys. Rev. B* **84**, 094503 (2011).
- ³³ A. Joshua, S. Pecker, J. Ruhman, E. Altman, and S. Ilani, ArXiv e-prints (2011), [arXiv:1110.2184](https://arxiv.org/abs/1110.2184).
- ³⁴ M. Breitschaft, V. Tinkl, N. Pavlenko, S. Paetel, C. Richter, J. R. Kirtley, Y. C. Liao, G. Hammerl, V. Eyert, T. Kopp, and J. Mannhart, *Phys. Rev. B* **81**, 153414 (2010).
- ³⁵ N. Pavlenko, T. Kopp, E. Y. Tsymbal, G. A. Sawatzky, and J. Mannhart, *Phys. Rev. B* **85**, 020407 (2012).
- ³⁶ P. Delugas, A. Filippetti, V. Fiorentini, D. I. Bilc, D. Fontaine, and P. Ghosez, *Phys. Rev. Lett.* **106**, 166807 (2011).
- ³⁷ M. Salluzzo, J. C. Cezar, N. B. Brookes, V. Bisogni, G. M. de Luca, C. Richter, S. Thiel, J. Mannhart, M. Huijben, A. Brinkman, G. Rijnders, and G. Ghiringhelli, *Physical Review Letters* **102**, 166804 (2009).
- ³⁸ J. Mannhart, D. Blank, H. Hwang, A. Millis, and J.-M. Triscone, *MRS bulletin* **33**, 1027 (2008).
- ³⁹ M. Lee, J. R. Williams, S. Zhang, C. D. Frisbie, and D. Goldhaber-Gordon, *Physical Review Letters* **107**, 256601 (2011).
- ⁴⁰ S. R. White, *Phys. Rev. Lett.* **69**, 2863 (1992).
- ⁴¹ T. Giamarchi, *Quantum physics in one dimension* (Oxford University Press, 2004).
- ⁴² M. Wimmer, A. R. Akhmerov, M. V. Medvedyeva, J. Tworzydło, and C. W. J. Beenakker, *Phys. Rev. Lett.* **105**, 046803 (2010).
- ⁴³ A. C. Potter and P. A. Lee, *Phys. Rev. Lett.* **105**, 227003 (2010).
- ⁴⁴ R. M. Lutchyn, T. D. Stanescu, and S. Das Sarma, *Phys. Rev. Lett.* **106**, 127001 (2011).
- ⁴⁵ G. Cheng, J. P. Veazey, P. Irvin, C. Cen, D. F. Bogorin¹, F. Bi, M. Huang, S. Lu, C.-W. Bark, S. Ryu, K.-H. Cho, C.-B. Eom, and J. Levy, "Evidence for topologically protected transport in sketched oxide nanostructures," (2012).
- ⁴⁶ S. Thiel, G. Hammerl, A. Schmehl, C. W. Schneider, and J. Mannhart, *Science* **313**, 1942 (2006).
- ⁴⁷ P. Moetakef, J. R. Williams, D. G. Ouellette, A. Kajdos, D. Goldhaber-Gordon, S. J. Allen, and S. Stemmer, (2012), [arXiv:1204.1081](https://arxiv.org/abs/1204.1081).
- ⁴⁸ J. Levy, (2012), private Communication.